

THE FLORIDA STATE UNIVERSITY
COLLEGE OF ARTS AND SCIENCES

ANALYSIS OF REMOTELY FORCED OCEANIC
ROSSBY WAVES OFF CALIFORNIA

By

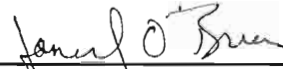
JAY F. SHRIVER

A Thesis Submitted to the
Department of Meteorology in partial
fulfillment of the requirements for
the degree of Masters of Science

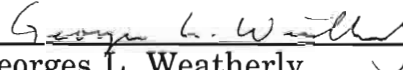
Degree Awarded:

Fall Semester, 1989

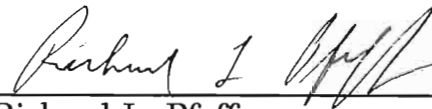
The members of the Committee approve the thesis of Jay F. Shriver defended on November 7, 1989.



James J. O'Brien
Professor Directing Thesis



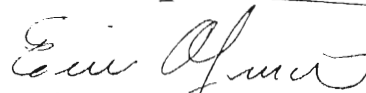
Georges L. Weatherly
Outside Committee Member



Richard L. Pfeffer
Committee Member



Paul H. Ruscher
Committee Member



Eric A. Smith
Committee Member

Abstract

Propagating principal component analysis (PPCA) is used to investigate the coastal Kelvin wave driven Rossby wave response in the northeast Pacific. Using PPCA, a spatial structure function is obtained from model upper layer thickness (ULT) data. The model used is a nonlinear, reduced gravity model of the northeast Pacific forced by coastal Kelvin wave propagation. The spatial structure function is used to extract the interannual Rossby wave response from 300 meter depth temperature anomalies. The observed Rossby wave signal is termed the projection mode.

The Rossby wave-like features observed in the projection mode are order 1000 km long with a majority of their periods ranging between 2 and 4 years. The wavenumbers and frequencies found are consistent with Rossby dynamics. The mean phase speed of the Rossby wave-like features within the projection mode is -1.3 cm sec^{-1} , in agreement with the theoretical Rossby wave phase speed at 40N. Large amplitude nearshore and decreasing amplitude away from shore suggests nearshore generation of these waves.

An important source of sea level variability along the west coast of North America at periods of 2-4 years was identified by Pares-Sierra and O'Brien (1989) as poleward propagating Kelvin waves. Since the Rossby wave-like features observed in the projection mode have a majority of O'Brien (1989) as poleward propagating Kelvin waves. Since the Rossby wave-like features observed in the projection mode have a majority of

their periods ranging between 2 and 4 years, their forcing can be attributed to long period Kelvin waves.

Spectral comparisons between the nearshore values in the projection mode and coastal sea level show greater than 90% coherence in the period band 3-4.4 years. The high coherence between coastal sea level variations and the projection mode shows that there is a strong correlation between the Rossby wave-like features within the projection mode and coastal Kelvin wave propagation.

It is concluded that the Rossby waves within the projection mode are forced by coastal Kelvin wave propagation. The projection mode accounts for 47.5% of the variance in the 300 meter depth temperature anomalies. The implication of this result is that the physical mechanism of the numerical model used, Rossby waves excited by coastal Kelvin wave propagation, accounts for 47.5% of the variance in the 300 meter depth temperature anomalies.

Dedication

On October 13, 1989 one of the original members of my supervisory committee, Dr. Thomas A. Carney died as a result of a prolonged illness. I would like to dedicate this thesis to his memory.

Acknowledgements

I would like to express my sincere gratitude to Dr. James J. O'Brien, the man who made it possible for me to come to Florida State. His guidance and support during this project was one of the keys to this project's success. Special thanks also to Dr. Mark A. Johnson, my right hand man on this project and the other key to the project's success. I would also like to thank professors Georges Weatherly, Paul Ruscher, Eric Smith and Richard Pfeffer for taking the time to be a part of my supervisory committee.

A special word of thanks to Dr. Albert Barcilon for noticing a significant calculation error and for taking the time to explain the mistake to me. Fortunately, the new calculations did not invalidate the conclusions based on the old calculations.

In addition, sincere appreciation is extended to my colleagues in the Mesoscale Air-Sea Interaction Group for always making me feel welcome and making my stay here in Tallahassee a pleasant one.

Finally, I would be remiss if I did not thank my parents. I could never thank them enough for all they've done for me.

Table of Contents

	Page
ABSTRACT	iii
DEDICATION	v
ACKNOWLEDGEMENTS	vi
TABLE OF CONTENTS	vii
LIST OF FIGURES	viii
1. INTRODUCTION	1
2. DATA	
2.1 OCEANIC	5
2.2 MODEL	7
3. PROPAGATING PRINCIPAL COMPONENT ANALYSIS	
3.1 MATHEMATICAL DEFINITION	13
3.2 TEST CASE	17
3.3 CALIFORNIA EXAMPLE	20
4. RESULTS AND DISCUSSION	26
5. SUMMARY AND CONCLUSIONS	37
REFERENCES	40

List of Figures

- | | Page |
|---|------|
| Figure 1. The 300 meter depth temperature data from April-May 1979. Variations in the main thermocline are reflected in temperatures at 300 meters depth. Warm temperatures generally correspond to a deep thermocline and cooler temperatures to a shallower thermocline. | 6 |
| Figure 2. Contours of temperature anomalies (in degrees Celsius) along 40N at 300 meters depth for 135W to 125W. Note the way the contours are sloping, implying westward motion, particularly during late 1983 through 1984. This westward motion can be interpreted as Rossby wave propagation and the Rossby wave activity in 1983-84 corresponds to the 1982-83 equatorial El Niño. | 8 |

- Figure 3. The domain of the equatorial model (Kubota and O'Brien, 1988) used to force the northeast Pacific model. Values of U, V and H were taken from a 15 degree transect at 18N and were imposed on the northeast Pacific model's southern boundary. (after Pares-Sierra and O'Brien, 1989) 11
- Figure 4. Contours of model ULT (in meters) with the overall mean removed. The waves are propagating at a phase speed of approximately 1.5 cm sec^{-1} . The maximum amplitude occurs on the boundary which indicates wave dispersion. 12
- Figure 5. The real (a.) and imaginary (b.) components of the test case SF. Note the wave number 2 pattern in both pictures and the $\frac{\pi}{2}$ shift of the curves. The wave number 2 pattern in space is consistent with the test function's wave number. The $\frac{\pi}{2}$ shift is a result of Hilbert transforming the data prior to complex EOF analysis. 19

	Page
Figure 6. Contours of model ULT (in meters) with the time mean for each space and space mean for each time of the data shown in Fig. 4 removed.	22
Figure 7. Contours of model eigenmode 1 ULT (in meters) accounting for 69.2% of the variance. Note the sloping lines which indicative of Rossby wave propagation. The large positive ULT anomalies in early 1977 and early 1983 through 1985 are both results of the equatorial El Niño events in 1976 and 1982-83. El Niño events are identified by anomalously warm ocean temperatures, or equivalently, anomalously large positive ULT.	23
Figure 8. Projection mode (values are in degrees Celsius). Rossby wave propagation is evident along with particularly large temperature anomalies in late 1976 - early 1977 and 1982-83. These large temperature anomalies are related to equatorial El Niño events in late 1976 - early 1977 and 1982-83.	27
Figure 9. The real (a.) and imaginary (b.) components of	
Figure 9. The real (a.) and imaginary (b.) components of the model eigenmode 1 spatial function.	28

	Page
Figure 10. The real (a.) and imaginary (b.) components of the projection temporal function.	29
Figure 11. An x-t picture of amplitude contribution with the overall mean removed (values are in degrees Celsius) formed by multiplying the amplitude functions of the vectors in Figs. 9 and 10. Note decreasing amplitude contribution away from shore, indicative of wave dispersion. Note also large amplitude contributions in late 1977 and 1983, both related to equatorial El Niño activity.	30
Figure 12. Wavelength (in kilometers) of the Rossby waves observed within the projection mode versus longitude. The wavelengths are order 1000 km, generally increasing offshore.	31

Figure 13. The frequencies (in cycles year⁻¹) of the Rossby waves observed within the projection mode versus time. A majority of the frequencies range between -.5 and -.25 cycles year⁻¹, corresponding to periods between 2 and 4 years. 33

Figure 14. Coherence of the PMC and coastal sea level at San Francisco. Note the 90% or greater coherence in the period band 3-4.4 years. The spectra has been Hanning smoothed, resulting in a loss of coherence values at the frequency extremes. 35

1. Introduction

El Niño events of varying intensity occur in the equatorial Pacific and have been documented as far back as 1525 by Quinn and Neal (1987). According to the hypothesis put forth by Wyrtki (1975), El Niño is a response of the equatorial Pacific Ocean to atmospheric forcing. In the tropical Pacific, prior to the onset of El Niño, strong southeast trades exist over the central Pacific. The result of the strong trades is an accumulation of water in the western equatorial Pacific, increasing the east-west sea level slope. Relaxation of the trades results in the accumulated water travelling eastward in the form of a downwelling equatorial Kelvin wave.

El Niño events have both oceanic and atmospheric implications. The downwelling equatorial Kelvin wave acts to suppress upwelling, shutting off a source of nutrient rich water and hence upsetting the ocean's biological balance off Peru. With the reduced upwelling, anomalously warm ocean temperatures result. El Niño events are thought to cause decreased hurricane activity in the Atlantic, droughts in southeast Asia, floods in Brazil, and many other anomalous weather conditions (O'Brien, 1987). Because El Niño is such a large scale equatorial event, it is natural to ask whether it has a significant midlatitude influence. Is equatorial El Niño information communicated through the ocean to midlatitudes, i.e., does an oceanic teleconnection midlatitude influence. Is equatorial El Niño information communicated through the ocean to midlatitudes, i.e., does an oceanic teleconnection exist between the equatorial and so called midlatitude El Niño?

The equatorial Kelvin wave, upon impinging on the west coast of Peru, has been shown in theoretical work to be able to generate poleward propagating coastal Kelvin waves (Moore, 1968; Anderson and Rowlands, 1976; Clarke, 1983). Poleward propagating Kelvin waves along the west coast of North America have been shown to excite Rossby waves in numerical work by White and Saur (1983), Pares-Sierra and O'Brien (1989) and Johnson and O'Brien (1989).

First mode baroclinic Rossby waves account for a significant portion of the mesoscale variability in the midlatitude eastern Pacific (Emery and Magaard, 1976; Price and Magaard, 1980, 1983). In addition to Rossby waves generated by coastal Kelvin wave propagation, Rossby waves can also be generated by wind stress curl forcing (White, 1982, 1985; White and Saur, 1981, 1983; Pares-Sierra and O'Brien, 1989). In order to investigate further these oceanic teleconnections, this research focuses on Rossby waves forced by coastal Kelvin wave propagation along the west coast of North America.

A nonlinear, reduced gravity, $1\frac{1}{2}$ layer model (discussed in 2.2) is used to simulate the oceanic circulation in the northeast Pacific in order to test the hypothesis of an oceanic teleconnection. This type of simple model has been used successfully in the equatorial Pacific (Inoue and O'Brien, 1987; Kubota and O'Brien, 1988). Kelvin waves propagating northward along the west coast of North America are used as the forcing. Model simulations show Rossby waves radiating westward from the west coast of North America as far north as 50N, the northern forcing. Model simulations show Rossby waves radiating westward from the west coast of North America as far north as 50N, the northern boundary of the model.

The goal of this paper is to demonstrate and validate that the physical mechanism of the numerical model is present in the midlatitude Pacific. Evidence will also be presented to support the existence of an oceanic teleconnection. A mathematical technique called propagating principal component analysis (PPCA) will be used. PPCA can extract physical information describing the varying physical attributes of propagating features in travelling wave-like fields.

Through the use of PPCA a spatial structure function is obtained from model upper layer thickness (ULT) data. The spatial structure function is used to extract the coastal Kelvin wave excited Rossby wave signal from 300 meter depth oceanic temperature anomalies. Rossby waves generated by coastal Kelvin wave propagation are shown to account for 47.5% of the variance in 300 meter depth temperature anomalies. The implication of this result is that the physical mechanism of the numerical model used in this research thereby accounts for 47.5% of the variance in the temperature anomalies. The Rossby waves have wavelengths on the order of 1000 km and a majority of their periods ranging between 2 and 4 years.

This analysis focuses on the longitude band 135W-125W at 40N. Due to its dispersive nature, the Rossby wave signal is anticipated to be strongest nearshore. Thus, a 10 degree longitude band, 135W-125W, was chosen for the analysis. 40N was chosen for the analysis since the greatest density of oceanic temperature values was found at this latitude.
greatest density of oceanic temperature values was found at this latitude.

The next section discusses in detail the oceanic and model data used in this research. Section 3 first defines PPCA and then illustrates its utility by presenting a test case. Next is a discussion of how PPCA is used to extract the coastal Kelvin wave excited Rossby wave signal from the 300 meter depth temperature data. Section 4 concludes with a derivation showing how to obtain frequency and amplitude information from the Rossby wave signal obtained through PPCA. The remaining sections present and discuss our results.

2. Data

2.1. *oceanic*

The oceanic data used in this study was furnished by Warren White, Scripps Institution of Oceanography, San Diego, California. The data consists of expendable bathythermograph (XBT) temperatures at 300 meters depth in the Pacific Ocean for the domain 30N to 50N and 130E to 120W, roughly the entire north Pacific Ocean. The data was collected through the TRANSPAC Volunteer Observing Ship program. The temperatures are gridded into $\frac{1}{2}$ degree by $\frac{1}{2}$ degree values in space and are gridded bimonthly in time for the period June-July 1976 to October-November 1984. The 300 meter temperature field for April-May 1979 is shown in Fig. 1. Temperature variability at 300 meters is indicative of fluctuations in the main thermocline. Warm temperatures generally correspond to a deep thermocline and cooler temperatures to a shallower thermocline.

In the present analysis we remove the time mean for each bimonth to eliminate the annual signal, leaving signals with interannual time scales, hence signals of propagating Rossby waves with interannual time scales should remain. Prior to mean calculation and removal, the missing values in the temperature data were filled using linear interpolation in time, then the data were smoothed twice in both directions using 1-2-1 weighting Hanning passes. After mean removal it was determined that additional smoothing was necessary, so

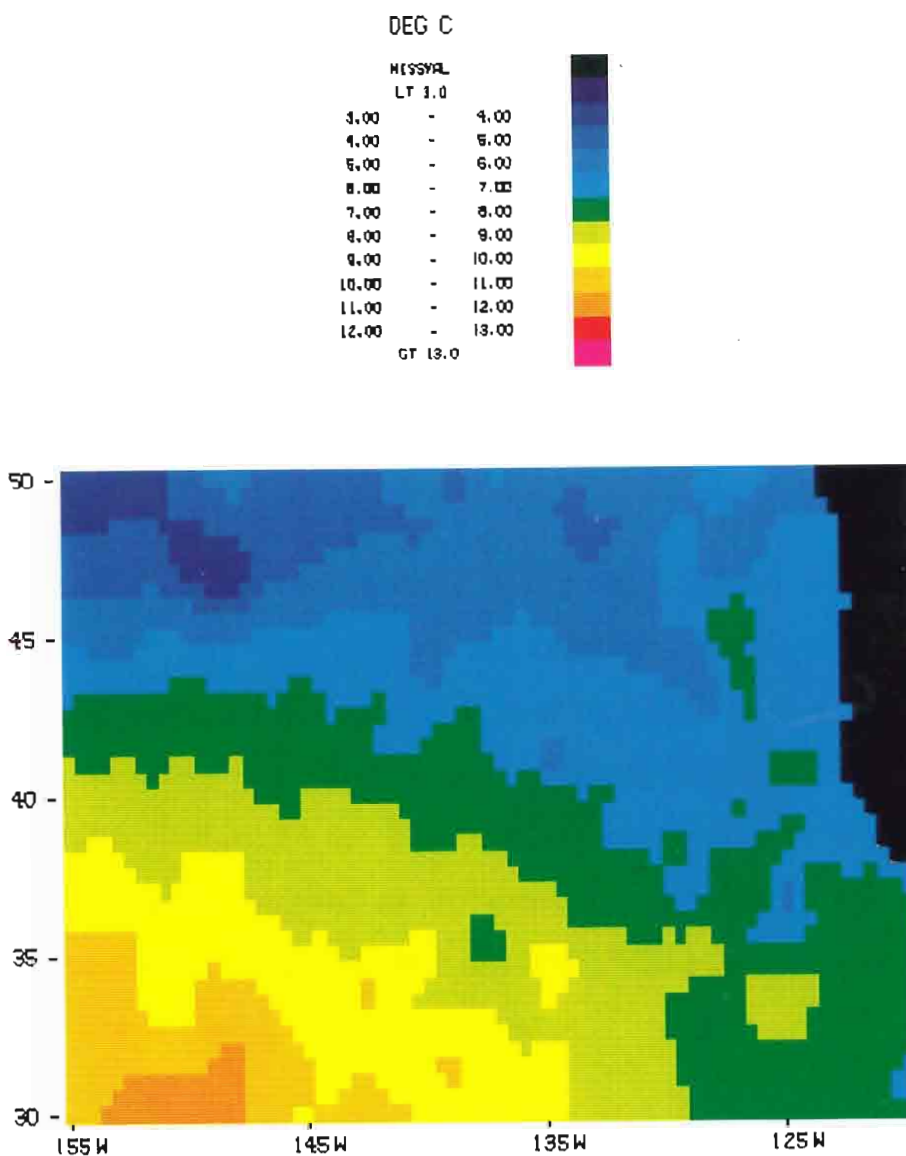


Figure 1. The 300 meter depth temperature data from April-May 1979. Variations in the main thermocline are reflected in temperatures at 300 meters depth. Warm temperatures generally correspond to a deep thermocline and cooler temperatures to a shallower thermocline.

the temperature anomalies were smoothed using 2 1-2-1 Hanning passes.

Temperature anomalies (bimonthly means removed) at 40N for the longitude band 135W-125W during the full time period are contoured in Fig. 2. Note the sloping contours, implying westward motion, particularly during late 1983 through 1984. This westward motion is indicative of Rossby wave propagation and the Rossby wave activity in 1983-84 corresponds to the 1982-83 equatorial El Niño.

2.2. model

A nonlinear reduced gravity model in spherical coordinates is used to simulate the variability in the northeast Pacific due to coastal Kelvin wave propagation. The model consists of one dynamically active layer of a density ρ and depth H on top of an infinitely deep layer of slightly higher density $\rho + \Delta\rho$. The interface between these two layers is a proxy of the ocean pycnocline. Spherical coordinates are used due to the latitudinal extent of the model (30N-50N). The equations defining the model are (Pares-Sierra and O'Brien, 1989),

$$\begin{aligned} \frac{\partial U}{\partial t} + \frac{1}{a \cos\theta} \frac{\partial}{\partial \phi} \left(\frac{U^2}{H} \right) + \frac{1}{a} \frac{\partial}{\partial \theta} \left(\frac{UV}{H} \right) - (2\Omega \sin\theta)V \\ = - \frac{g'}{2a \cos\theta} \frac{\partial H^2}{\partial \phi} + AV^2U \end{aligned} \quad (1a)$$

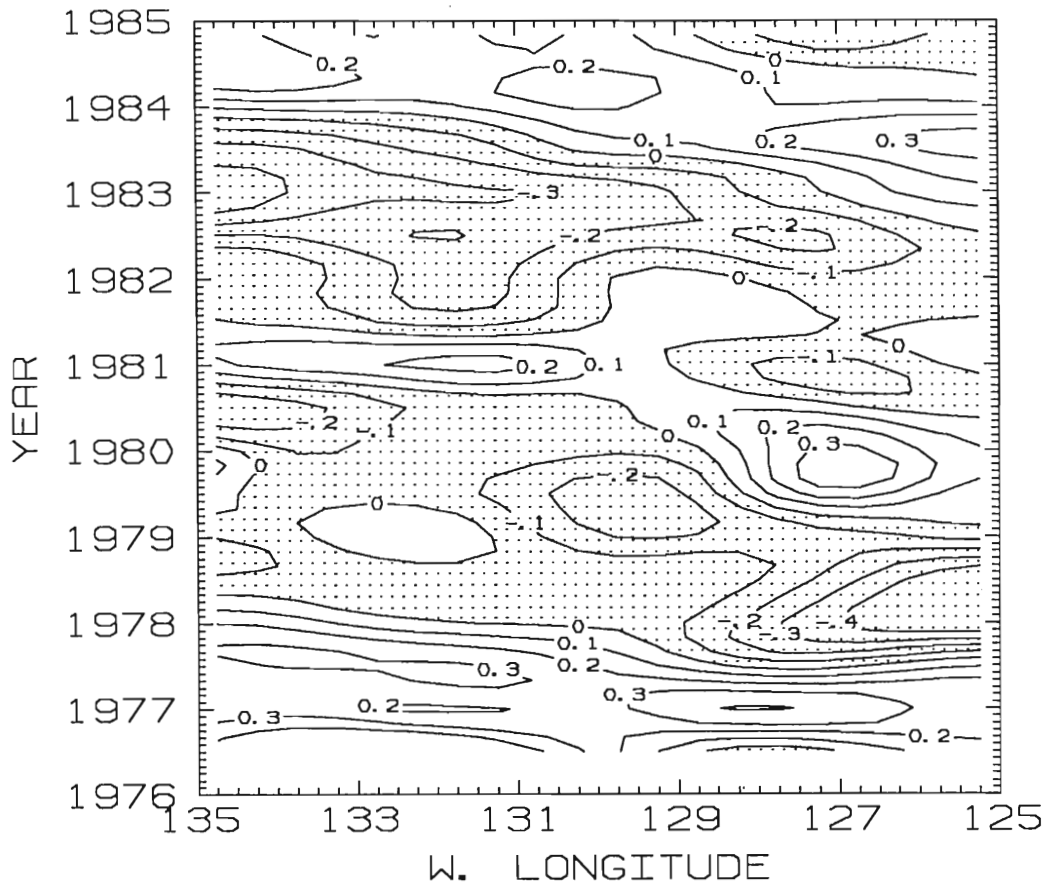


Figure 2. Contours of temperature anomalies (in degrees Celsius) along 40N at 300 meters depth for 135W to 125W. Note the way the contours are sloping, implying westward motion, particularly during late 1983 through 1984. This westward motion can be interpreted as Rossby wave propagation and the Rossby wave activity in 1983-84 corresponds to the 1982-83 equatorial El Niño.

$$\begin{aligned} \frac{\partial V}{\partial t} + \frac{1}{a \cos \theta} \frac{\partial}{\partial \phi} \left(\frac{UV}{H} \right) + \frac{1}{a} \frac{\partial}{\partial \theta} \left(\frac{V^2}{H} \right) + (2\Omega \sin \theta)U \\ = -\frac{g'}{2a} \frac{\partial H^2}{\partial \theta} + A \nabla^2 V \end{aligned} \quad (1b)$$

$$\frac{\partial H}{\partial t} + \frac{1}{a \cos \theta} \left(\frac{\partial U}{\partial \phi} + \frac{\partial}{\partial \theta} (V \cos \theta) \right) = 0 \quad (1c)$$

where ϕ and θ are the longitude and latitude, respectively; U and V are the transport in the east-west and north-south directions, respectively; H is the depth of the upper layer; $g'=(\Delta\rho/\rho)g$ is the reduced gravity; A is an eddy viscosity coefficient; a is the radius of the earth; and Ω is the angular velocity of rotation of the earth.

Equations (1 a-c) were solved for the domain 18N to 50N and from 155W to the west coast of North America. The equations were discretized into a staggered grid (Arakawa C-grid). A one twelfth of a degree resolution was used in both the zonal and meridional directions (defined as the U to H distance in the staggered grid), with integration time steps of 20 minutes. The eastern boundary has a no-slip condition ($U=V=0$). The north, south and west boundaries are open boundaries, employing a numerically implemented Sommerfeld radiation condition (see Camerlengo and O'Brien, 1980).

The model was forced at the eastern edge of the southern boundary by imposing the results of a wind forced, reduced gravity equatorial model (Kubota and O'Brien, 1988) in order to test the hypothesis that remotely excited Rossby waves play a major role in the equatorial model (Kubota and O'Brien, 1988) in order to test the hypothesis that remotely excited Rossby waves play a major role in the midlatitude El Niño response. That model domain encompassed the

equatorial Pacific from 20S to 25N and was run from January 1961 to December 1984. U, V, and H were taken from this model along a 15 degrees longitude band at 18N, and were used to force the above model (see Fig. 3).

The width of the southern boundary used for forcing had to be wide enough to allow coastally trapped waves to propagate through, but it had to be narrow enough to minimize contamination of the interior due to reflection of waves at the forced southern boundary. A 15 degree length was selected for the forced boundary.

An x-t picture of model upper layer thickness (ULT) at 40N for 155W-125W and June-July 1976 - October-November 1984 with the overall mean removed is shown in Fig. 4. Rossby wave propagation is evident and the waves are propagating at a phase speed of approximately 1.5 cm sec^{-1} .

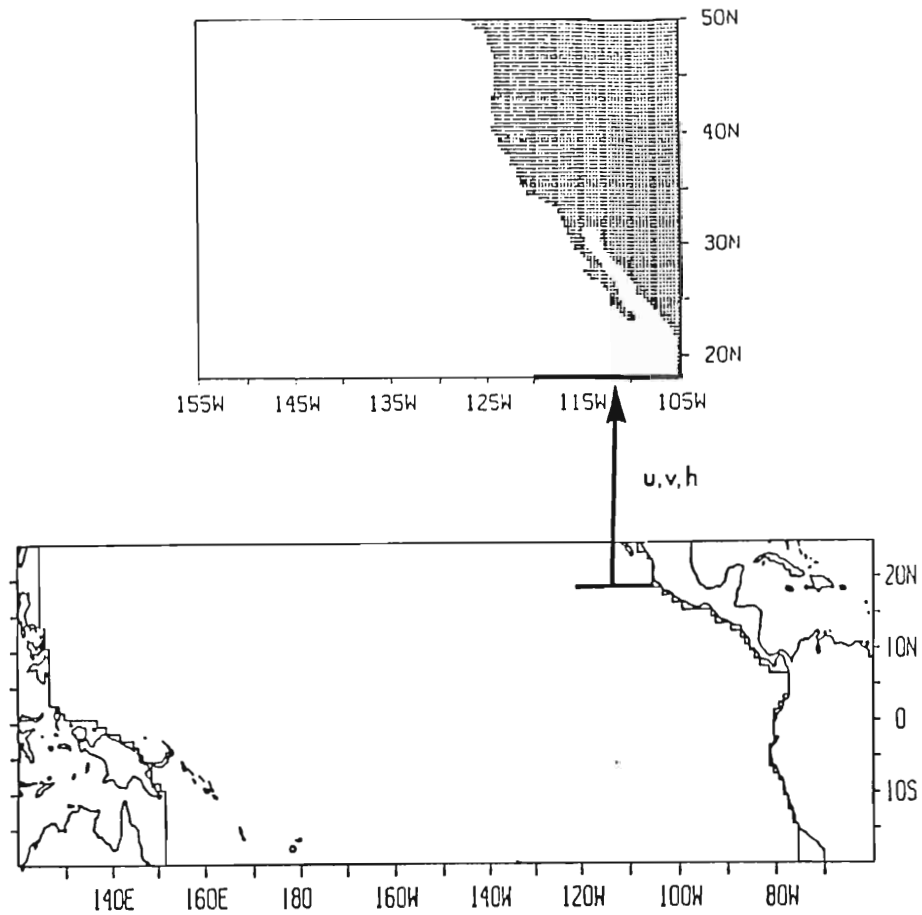


Figure 3. The domain of the equatorial model (Kubota and O'Brien, 1988) used to force the northeast Pacific model. Values of U , V and H were taken from a 15 degree transect at 18N and were imposed on the northeast Pacific model's southern boundary. (after Pares-Sierra and O'Brien, 1989)

Values of U , V and H were taken from a 10 degree transect at 10N and were imposed on the northeast Pacific model's southern boundary. (after Pares-Sierra and O'Brien, 1989)

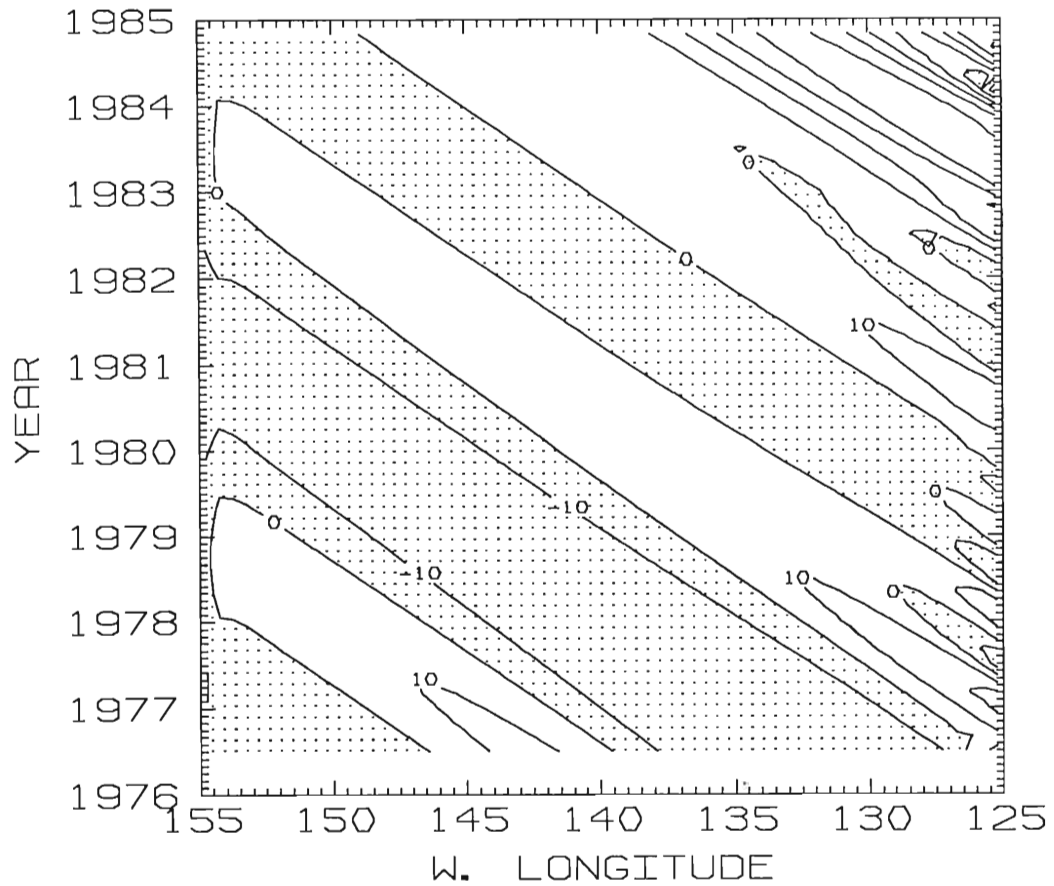


Figure 4. Contours of model ULT (in meters) with the overall mean removed. The waves are propagating at a phase speed of approximately 1.5 cm sec^{-1} . The maximum amplitude occurs on the boundary which indicates wave dispersion.

3. Propagating principal component analysis

3.1. mathematical definition

The goal of this technique (see Barnett, 1983; Priesendorfer, 1988) is to extract physical information on propagating features from a two dimensional data array

$$u = (u_{nm})_{N \times M},$$

where u is an $N \times M$ matrix with elements u_{nm} and N and M being the number of space and time points, respectively. Through the use of the Hilbert transform (to obtain phase and amplitude information) and complex empirical orthogonal function (EOF) analysis the component eigenmodes of u are obtained, each yielding wavenumber, frequency and amplitude information.

First the Hilbert transform is defined by

$$\hat{u}_{nm} = \sum_{\omega} [b_n(\omega) \cos(\omega t_m) - a_n(\omega) \sin(\omega t_m)], \quad (2.)$$

where $t_m = t_0 + m\Delta t$. Here, b_n and a_n can be determined from the Fourier series representation of u ,

$$u_{nm} = \sum_{\omega} [a_n(\omega) \cos(\omega t_m) + b_n(\omega) \sin(\omega t_m)],$$

$$u_{nm} = \sum_{\omega} [a_n(\omega) \cos(\omega t_m) + b_n(\omega) \sin(\omega t_m)],$$

so that a new complex array

$$U = u + i \hat{u} , \quad (3.)$$

where $i = \sqrt{-1}$, can be constructed.

By use of (2.) each Fourier component of \hat{u} is phase shifted by $\frac{\pi}{2}$ in time. Barnett (1983) notes that a $\frac{\pi}{2}$ phase shift of each Fourier component provides optimal lag information on that component. Thus, U contains information on relative phases. In addition to phase information, amplitude information can be extracted from U (Bendat and Piersol, 1986), and will be discussed fully later in this section.

Complex EOF analysis is used on U to partition its variance into component eigenmodes, each mode explaining a certain percentage of the variance of U . The more significant eigenmodes may have physical interpretations associated with them. The complex EOF analysis used here follows Legler (1983). The covariance matrix of U is given by

$$C = U^{*T}U,$$

where $*T$ denotes conjugate transpose. C is a Hermitian $M \times M$ matrix having real eigenvalues.

The eigenvector decomposition of C yields M real eigenvalues λ_i and M associated complex eigenvectors

and M associated complex eigenvectors

$$\mathbf{E}_i = (\mathbf{E}_m)_{1 \times M},$$

where \mathbf{E}_i is a $1 \times M$ vector with elements E_m . The set of M eigenvectors form an orthonormal basis from which the original data can be represented. The vector \mathbf{E}_i will be referred to as the temporal function (TF).

Through complex EOF analysis, U can be represented as the product of a temporal vector (in this case \mathbf{E}_i) and a corresponding spatial vector (\mathbf{W}_i) summed over M , i.e.

$$U = \sum_{i=1}^M \mathbf{W}_i \mathbf{E}_i,$$

where

$$\mathbf{W} = (\mathbf{W}_n)_{N \times 1}.$$

To solve for \mathbf{W} for a given i (eigenmode) right multiply both sides by \mathbf{E}_i^{*T} , yielding

$$\mathbf{W}_i = U \mathbf{E}_i^{*T}.$$

The vector \mathbf{W} will be referred to as the spatial function (SF).

Through this technique, U has been decomposed into its component eigenmodes, each of which account for a certain percentage of the variance of U , given by component eigenmodes, each of which account for a certain percentage of the variance of U , given by

$$[\text{variance explained by eigenmode } i] = \frac{\lambda_i}{\sum_{k=1}^M \lambda_k}.$$

Further, the phase and amplitude information has been similarly decomposed. As will be shown, it is possible to obtain phase and amplitude information from the spatial and temporal components respectively of a given eigenmode, yielding some very useful physical information as described below.

There are four functions which may describe physical attributes of moving features in u for a given eigenmode i (Barnett, 1983):

1.) *spatial amplitude function* $S_i(x)$

This function shows the variability of amplitude in space associated with a given eigenmode. $S_i(x)$ is defined as

$$S_i(x) = [W_i W_i^*]^{1/2},$$

where * denotes complex conjugate.

2.) *temporal amplitude function* $R_i(t)$

$R_i(t)$ is defined as

$$R_i(t) = [E_i E_i^*]^{1/2}.$$

$$R_i(t) = [E_i E_i^*]^{1/2}.$$

$\mathbf{R}_i(t)$ provides information on the temporal variability of amplitude.

3.) *spatial phase function* $\Theta_i(x)$

The spatial phase function $\Theta_i(x)$ shows the spatial variation of phase associated with u . $\Theta_i(x)$ is defined as

$$\Theta_i(x) = \arctan\left(\frac{\text{Im } \mathbf{W}_i}{\text{Re } \mathbf{W}_i}\right).$$

It is from this function that wave number information can be derived (as will be shown).

4.) *temporal phase function* $\phi_i(t)$

The temporal phase function $\phi_i(t)$ shows the temporal variation of phase associated with u and $\phi_i(t)$ is defined as

$$\phi_i(t) = \arctan\left(\frac{\text{Im } \mathbf{E}_i}{\text{Re } \mathbf{E}_i}\right).$$

Frequency information can be derived from $\phi_i(t)$ (to be discussed later).

3.2. *Test case*

Consider a traveling cosine wave with constant wave number, frequency and amplitude:

Consider a traveling cosine wave with constant wave number, frequency and amplitude:

$$f(x,t) = A\cos(kx-\omega t), \quad (4.)$$

where $x=1,2,3,\dots,64$ and $t=1,2,3,\dots,64$. For the function we choose amplitude, $A=2$, wavenumber, $k = 2\pi/32$ and frequency, $\omega = 2\pi/64$. An $x-t$ plot (not shown) of (4.) reveals a picture similar to the model ULT contours shown in Fig. 4, with evenly spaced contours having constant slopes equal to $\omega/k = 0.5$.

When the data defined by (4.) was processed using PPCA all of the variance was accounted for by the first eigenmode, hence the first eigenmode reproduces $f(x,t)$. The SF picture associated with $f(x,t)$ is shown in Fig. 5. There is a wave number 2 pattern evident in both the real and imaginary components of the SF picture, consistent with the given wavenumber. The $\frac{\pi}{2}$ shift is a direct result of Hilbert transforming the data prior to complex EOF analysis.

The TF picture is a wave number 1 pattern in time (consistent with the chosen ω) and displays a similar $\frac{\pi}{2}$ phase shift (except shifted in an opposite sense) between the real and imaginary components.

The more interesting features of PPCA are evident when the four functions (spatial amplitude, spatial phase, temporal amplitude, temporal phase) discussed in the previous section are calculated. Calculation of the spatial and temporal amplitude functions show that $S(x) = 16$ and $R(t) = .125$. Note that the amplitude contributions for the time and space components are constant. Further, if $S(x)$ and $R(t)$ are multiplied together, the amplitude of the first eigenmode in $x-t$ space is time and space components are constant. Further, if $S(x)$ and $R(t)$ are multiplied together, the amplitude of the first eigenmode in $x-t$ space is realized.

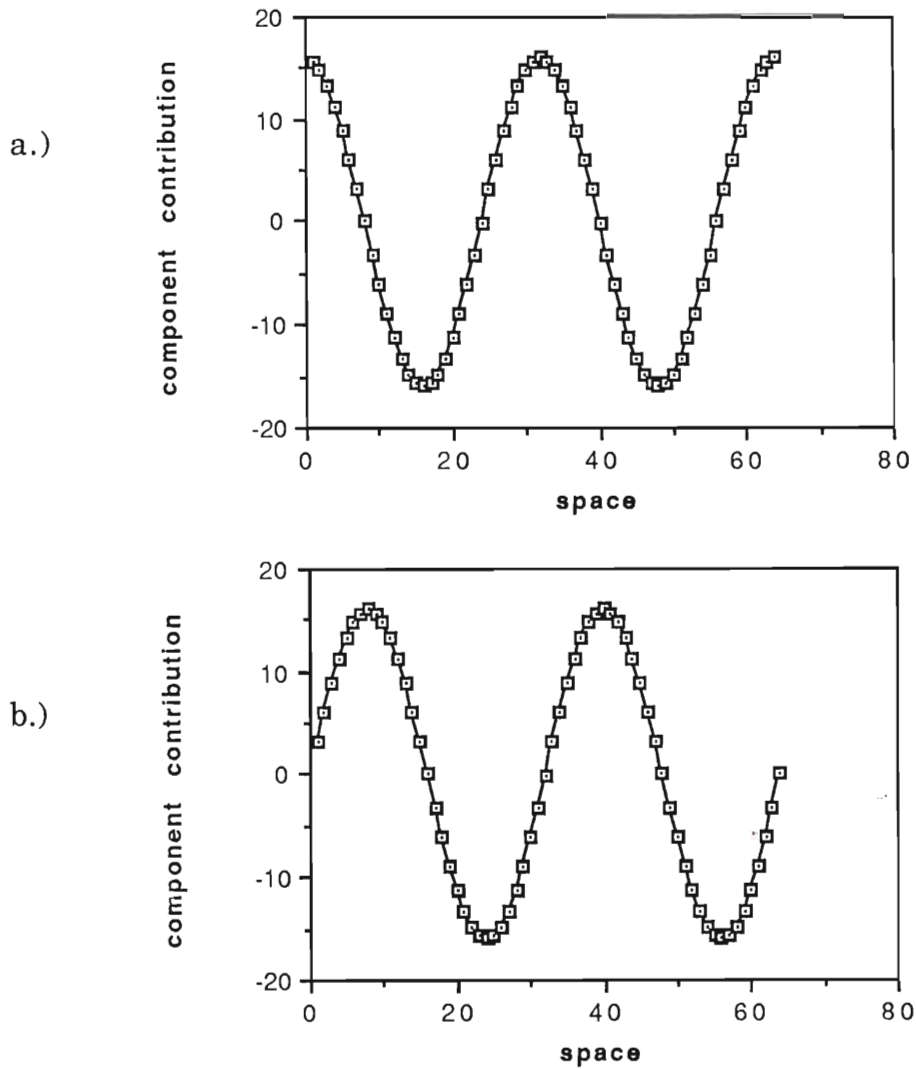


Figure 5. The real (a.) and imaginary (b.) components of the test case SF. Note the wave number 2 pattern in both pictures and the $\frac{\pi}{2}$ shift of the curves. The wave number 2 pattern in space is consistent with the test function's wave number. The $\frac{\pi}{2}$ shift is a result of Hilbert transforming the data prior to complex EOF analysis.

The spatial derivative of the spatial phase function yields the wavenumber,

$$\frac{\partial}{\partial x}(\Theta(x)) = .20 \cong \frac{2\pi}{32}.$$

The derivative of the temporal phase function yields the frequency,

$$\frac{\partial}{\partial t}(\phi(t)) = .10 \cong \frac{2\pi}{64}.$$

For this simple traveling wave case, the four functions discussed above yield the information needed to fully describe the physical attributes of the x-t field yielded by (4.).

3.3. *California example*

To examine the relationship between the model ULT and temperature anomalies, the correlation coefficient (r) was first calculated, yielding $r=16\%$. To further examine how well the two data sets correlated EOF analysis was used (identical to the technique described in 3.3, except that the matrix component obtained via the Hilbert transform is set to zero) to partition the ULT and temperature anomalies into component eigenmodes. EOF analysis has the ability to highlight predominant standing patterns. Correlations between the time components of the first three eigenmodes of the ULT and highlight predominant standing patterns. Correlations between the time components of the first three eigenmodes of the ULT and temperature anomalies yielded correlations of less than 25 percent. This

correlation of the time components is called canonical correlation (Priesendorfer, 1988). This technique is widely used in meteorology today. Due to the poor correlations PPCA was then used to help demonstrate the hypothesized relationship because PPCA is designed to extract physical information on moving features.

PPCA, as shown in the test case, is an effective tool for extracting information on propagating features. Since the features of interest in this research, Rossby waves, are propagating features, PPCA is the next logical choice for this analysis.

PPCA analysis requires that the data to be processed are demeaned, or else the variance of the first eigenmode will be artificially large. Prior to using PPCA on the model ULT data in Fig. 4, the space mean for each time and time mean for each space was removed yielding model ULT anomalies (Fig. 6). The model ULT anomalies in Fig. 6 are restricted to 135W-125W, the domain of interest. The space mean (for each time) that was removed was not for the longitude band 135W-125W, but for 155W-125W. The space mean for 135W-125W was first removed, but this caused the magnitude of the 1982-83 El Niño to be suppressed. However, the large El Niño magnitude was a feature of interest. Removing the space mean (for each time) based on values in the band 155W-125W left the magnitude of the 1982-83 El Niño large, so the space mean was removed in this way.

PPCA on the model ULT anomalies in Fig. 4 yielded 51 pairs of space and time vectors. The real part of eigenmode 1 was contoured for

PPCA on the model ULT anomalies in Fig. 4 yielded 51 pairs of space and time vectors. The real part of eigenmode 1 was contoured for inspection (see Fig. 7). It was clearly a Rossby-type mode (explaining

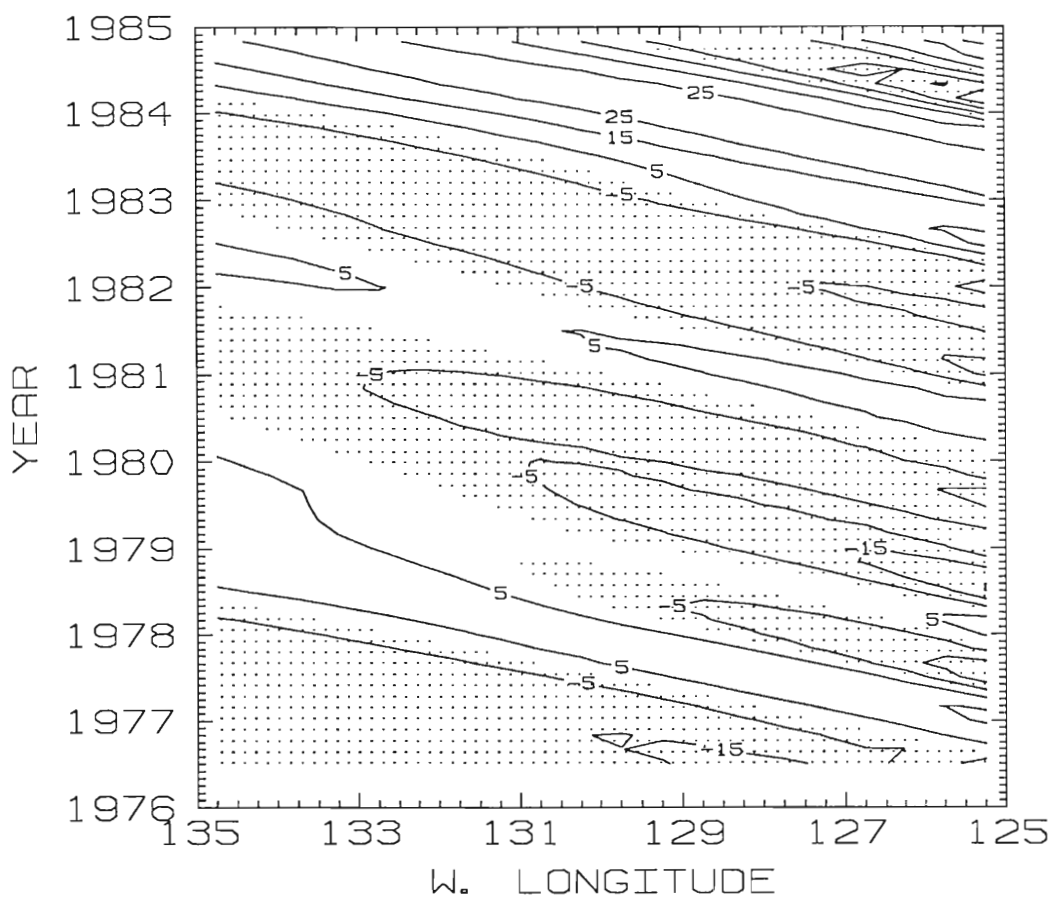


Figure 6. Contours of model ULT (in meters) with the time mean for each space and space mean for each time of the data shown in Fig. 4 removed.

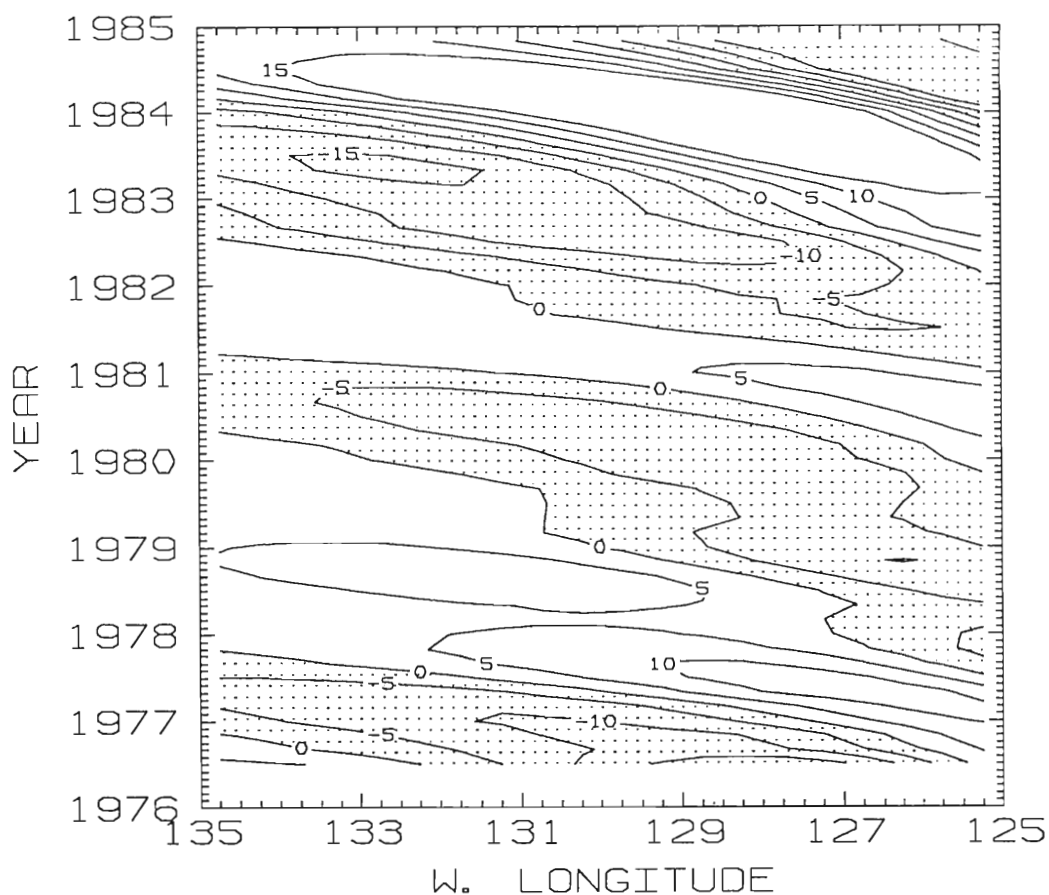


Figure 7. Contours of model eigenmode 1 ULT (in meters) accounting for 69.2% of the variance. Note the sloping lines which indicative of Rossby wave propagation. The large positive ULT anomalies in early 1977 and early 1983 through 1985 are both results of the equatorial El Niño events in 1976 and 1982-83. El Niño events are identified by anomalously warm ocean temperatures, or equivalently, anomalously large positive ULT.

69.2% of the variance), with sloping lines indicative of Rossby wave propagation. The next 4 eigenmodes accounted for 21.8, 7.2, 1.6 and .2 percent of the variance respectively. Eigenmodes 2-5 were contoured and found to have no identifiable Rossby wave-like features. Since the first eigenmode accounts for a significant portion of the variance and since the Rossby wave-like motion is confined to eigenmode 1, the following discussion is restricted to this mode.

To examine the coastal Kelvin wave forced Rossby wave signal in the 300 meter temperature data, a new data set was constructed and constrained to behave like the model Rossby wave signal spatially, and having its temporal variability determined from the temperature observations through

$$\mathbf{A} = \frac{\sum_n \mathbf{W}^{*T} D}{\sum_n \mathbf{W}^{*T} \mathbf{W}} \quad (5.)$$

where

$$\begin{aligned} \mathbf{W} &= (W_n)_{N \times 1} \\ \mathbf{A} &= (A_m)_{1 \times M} \\ D &= (D_{nm})_{N \times M}, \end{aligned}$$

Here, \mathbf{W} is the SF from model eigenmode 1, D is a complex array
 Here, \mathbf{W} is the SF from model eigenmode 1, D is a complex array formed according to (3.) where d is the 300 meter temperature anomaly data (Fig. 2) and N and M being the number of space and time points,

respectively. Equation (5.) extracts a temporal signal from D corresponding to the spatial signal from the model eigenmode 1. \mathbf{A} will be referred to as the projection temporal function (PTF). The product of \mathbf{W} and \mathbf{A} will yield what we will term the projection mode.

4. Results and discussion

PPCA yields wavenumber, frequency and amplitude information that describes the Rossby wave pattern in the projection mode. The projection mode is shown in Fig. 8. Rossby wave propagation is evident, with particularly large temperature anomalies in late 1976 - early 1977 and in 1982-83. These large temperature anomalies are related to equatorial El Niño events in late 1976 - early 1977 and 1982-83.

Figures 9 and 10 show the real (a) and imaginary (b) parts of the SF and PTF, respectively. When the SF and PTF amplitude functions are formed and multiplied to form a two dimensional amplitude field (Fig. 11), several attributes are evident. Due to Rossby wave dispersion, the amplitude field shows a decrease away from shore. The decreasing amplitude away from shore suggests nearshore generation of the observed waves. Temporally, large amplitude contributions are evident in 1977 and 1983, both related to equatorial El Niño activity. El Niño events are identified by anomalously warm ocean temperatures, reflected in large positive values in the amplitude field.

The wavelengths (as a function of space) of the features in the projection mode are shown in Fig. 12. Note the tendency for increase in the wavelength away from shore. Due to the dispersive nature of Rossby waves and since phase speed is a function of wavelength, faster phase speeds (longer waves) will be found near 135W and the slower phase speeds (shorter waves) will be found nearshore.

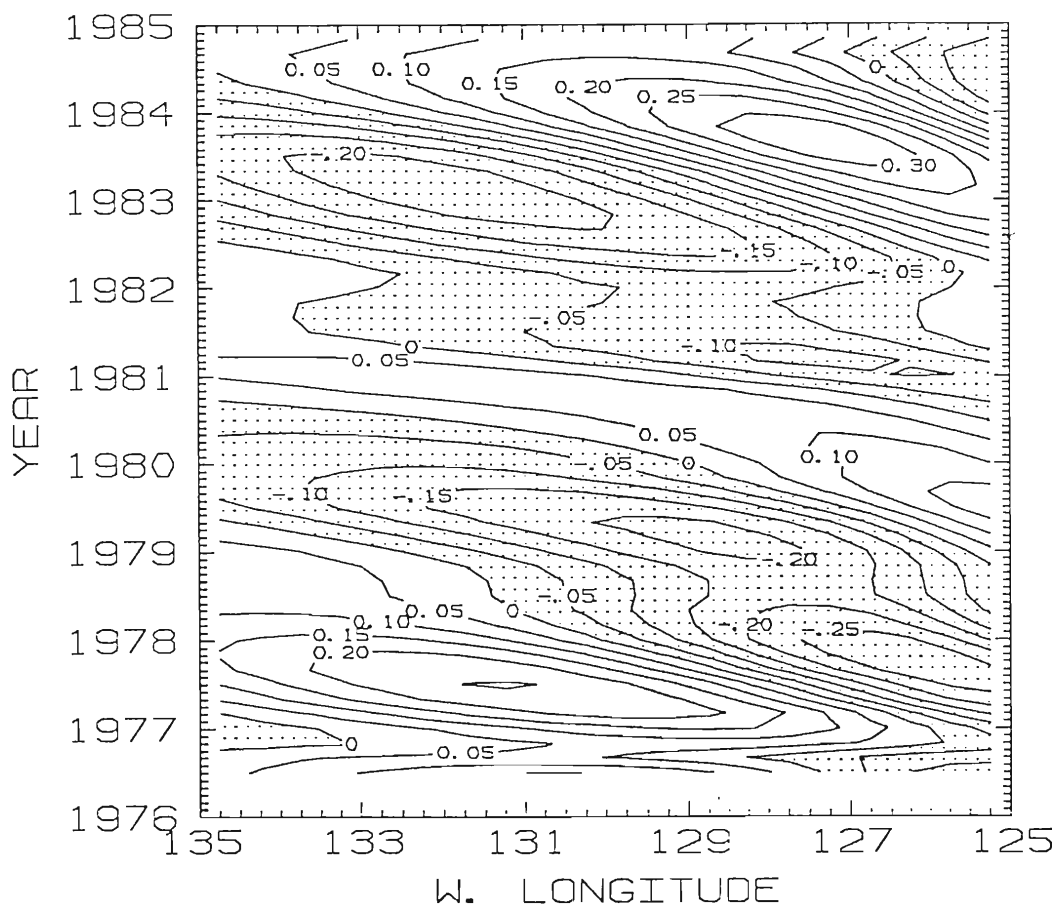


Figure 8. Projection mode (values are in degrees Celsius). Rossby wave propagation is evident along with particularly large temperature anomalies in late 1976 - early 1977 and 1982-83. These large temperature anomalies are related to equatorial El Niño events in late 1976 - early 1977 and 1982-83. These large temperature anomalies are related to equatorial El Niño events in late 1976 - early 1977 and 1982-83.

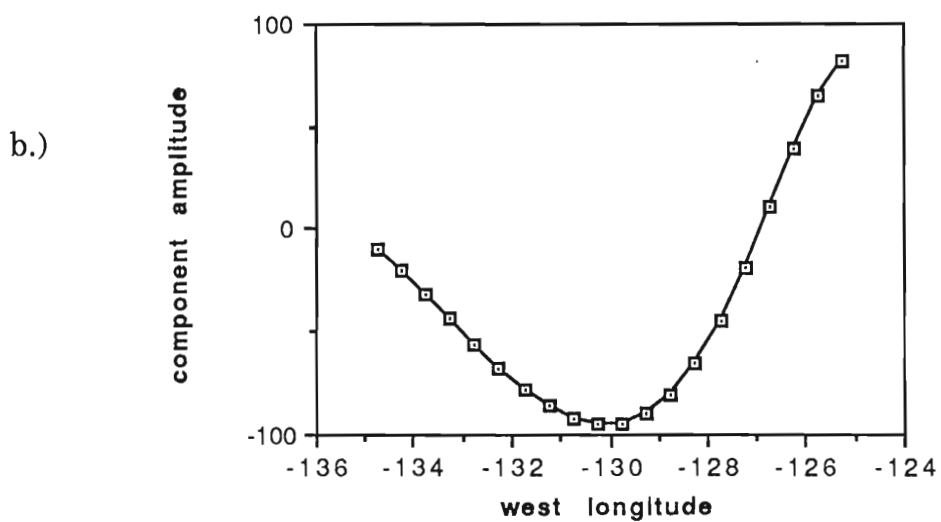
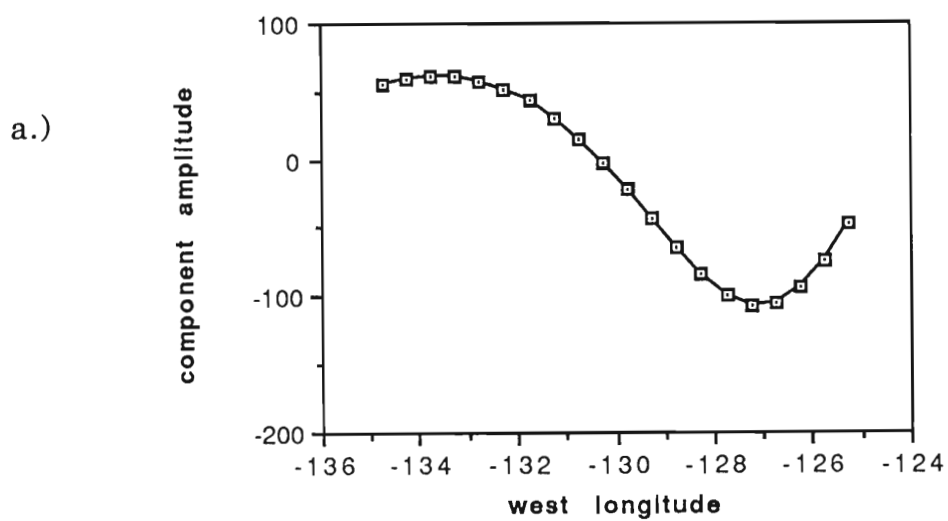


Figure 9. The real (a.) and imaginary (b.) components of the model

Figure 9. The real (a.) and imaginary (b.) components of the model eigenmode 1 spatial function.

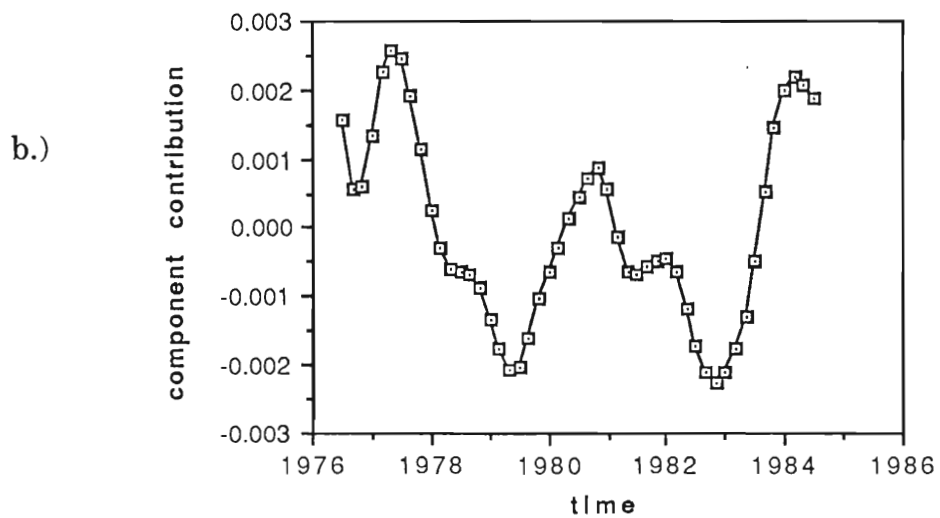
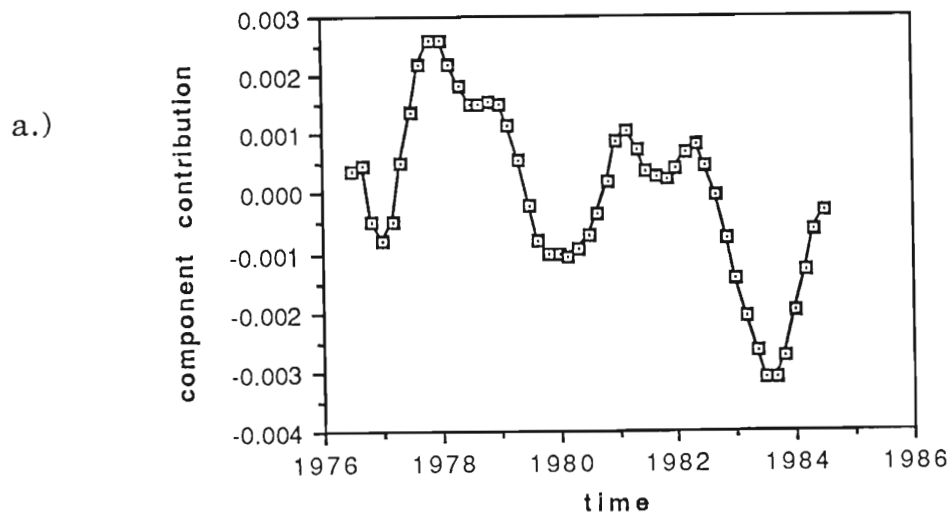


Figure 10. The real (a.) and imaginary (b.) components of the projection

Figure 10. The real (a.) and imaginary (b.) components of the projection temporal function.

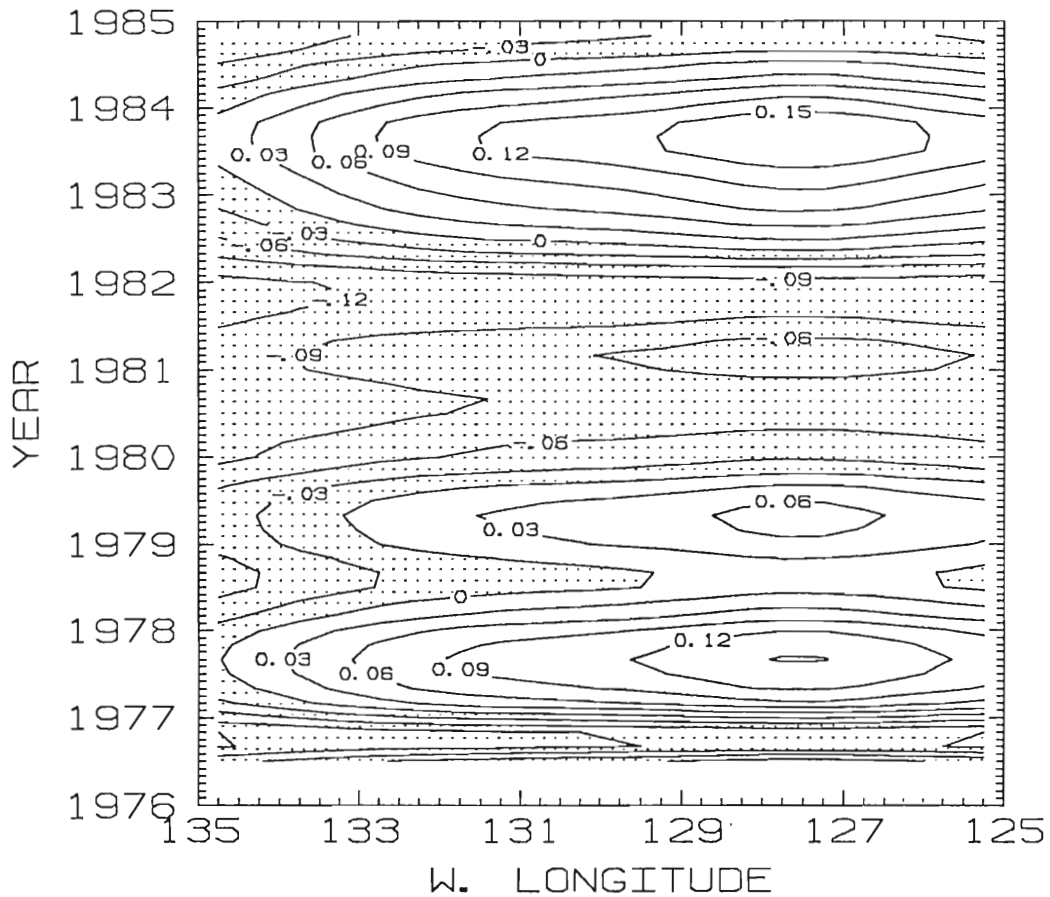


Figure 11. An x-t picture of amplitude contribution with the overall mean removed (values are in degrees Celsius) formed by multiplying the amplitude functions of the vectors in Figs. 9 and 10. Note decreasing amplitude contribution away from shore, indicative of wave dispersion. Note also large amplitude contributions in late 1977 and 1983, both related to equatorial El Niño activity.

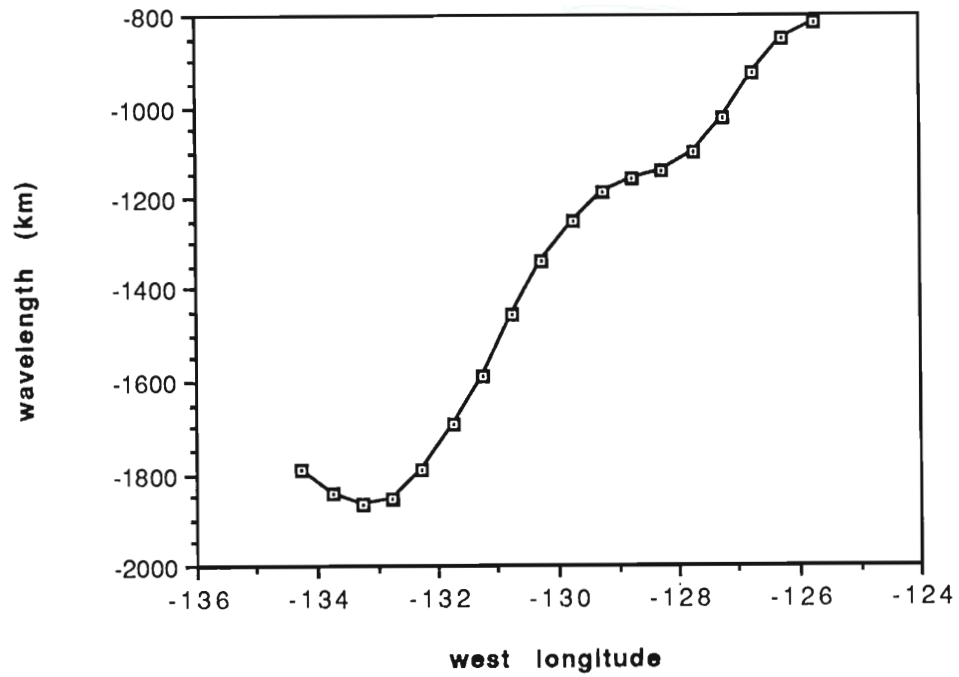


Figure 12. Wavelength (in kilometers) of the Rossby waves observed within the projection mode versus longitude. The wavelengths are order 1000 km, generally increasing offshore.

Finding features with wavelengths on the order of 1000 km in a 10 degree band of longitude at 40N (850km) at first seems suspect. This would be a major problem if wavelength information was obtained via spectral analysis, for example. The wavelengths in Fig. 12 were not found by fitting harmonics, rather they were computed directly from the spatial phase function. Therefore, the wavelength values in Fig.12 are not unreasonable, since they are not constrained by the limitations of fitting harmonics.

An important source of sea level variability along the west coast of North America at periods of 2-4 years was identified by Pares-Sierra and O'Brien (1989) as poleward propagating Kelvin waves. Figure 13 shows that a majority of the frequencies in the projection mode correspond to periods ranging between 2 and 4 years. Since observed frequencies are normally on the order of the forcing frequency, the forcing of Rossby wave-like features observed in the projection mode could be explained by poleward propagating Kelvin waves.

Additional evidence showing that coastal Kelvin waves excite Rossby waves can be found by comparing coastal sea level to the projection mode's value at 125W for the time period June-July 1976 - October-November 1984 (hereafter referred to as projection mode cut (PMC)). If the Rossby waves in the projection mode are indeed forced by coastal Kelvin wave propagation, a high degree of coherence can be expected in the period band attributed to poleward propagating Kelvin waves (2-4 years).
expected in the period band attributed to poleward propagating Kelvin waves (2-4 years).

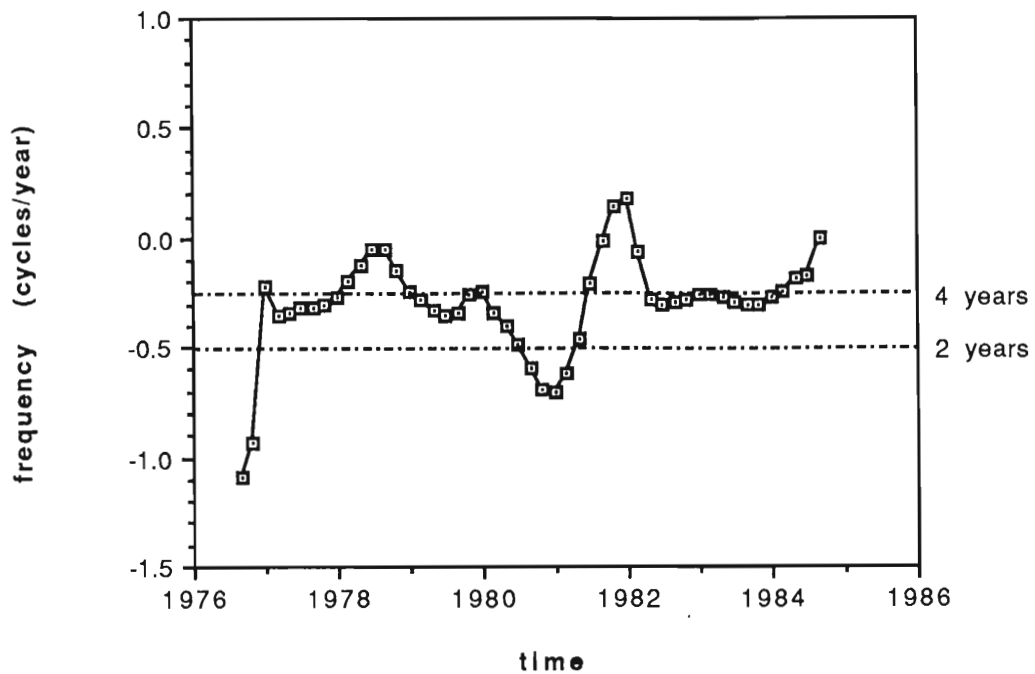


Figure 13. The frequencies (in cycles year⁻¹) of the Rossby waves observed within the projection mode versus time. A majority of the frequencies range between -0.5 and -0.25 cycles year⁻¹, corresponding to periods between 2 and 4 years.

Figure 14 shows the coherence between the PMC and coastal sea level at San Francisco. Note good coherence (above 90%) for the period band 1200 - 1600 days (3-4.4 years). The high degree of coherence between the PMC and coastal sea level at San Francisco in the period band 3-4.4 years shows that the PMC, hence the projection mode, is strongly correlated to coastal Kelvin waves.

The phase in the period band 3-4.4 years ranges from 11 to 28 degrees, with the PMC lagging coastal sea level. The average phase difference corresponds to an average phase error of approximately 100 days. Since 125W is approximately 1 degree offshore, it would seem reasonable to expect the two time series to be out of phase by some time related to the time it takes the Rossby waves to travel from their point of origin to 125W. The phase speed obtained by dividing 1 degree of longitude at 40N by 100 days is approximately 1 cm sec^{-1} (a reasonable phase speed, as will be discussed next). Thus, we expect that the phase difference is due to the time it takes the Rossby waves to travel from the point of generation to 125W.

The theoretical Rossby wave phase speed is $C = \omega/k = -\beta/(k^2 + (f/c)^2)$, where ω is the frequency defined by the Rossby wave dispersion relation (Gill, 1982, page 446), β is the meridional derivative of the Coriolis parameter f , k is the east-west local wavenumber and c is the gravity wave phase speed (2.5 m sec^{-1}). Using the mean wavenumber value from the projection mode (obtained by dividing 2π by the mean wavelength (from Fig. 12)), a mean theoretical phase speed of -1.2 cm sec^{-1} is from the projection mode (obtained by dividing 2π by the mean wavelength (from Fig. 12)), a mean theoretical phase speed of -1.2 cm sec^{-1} is

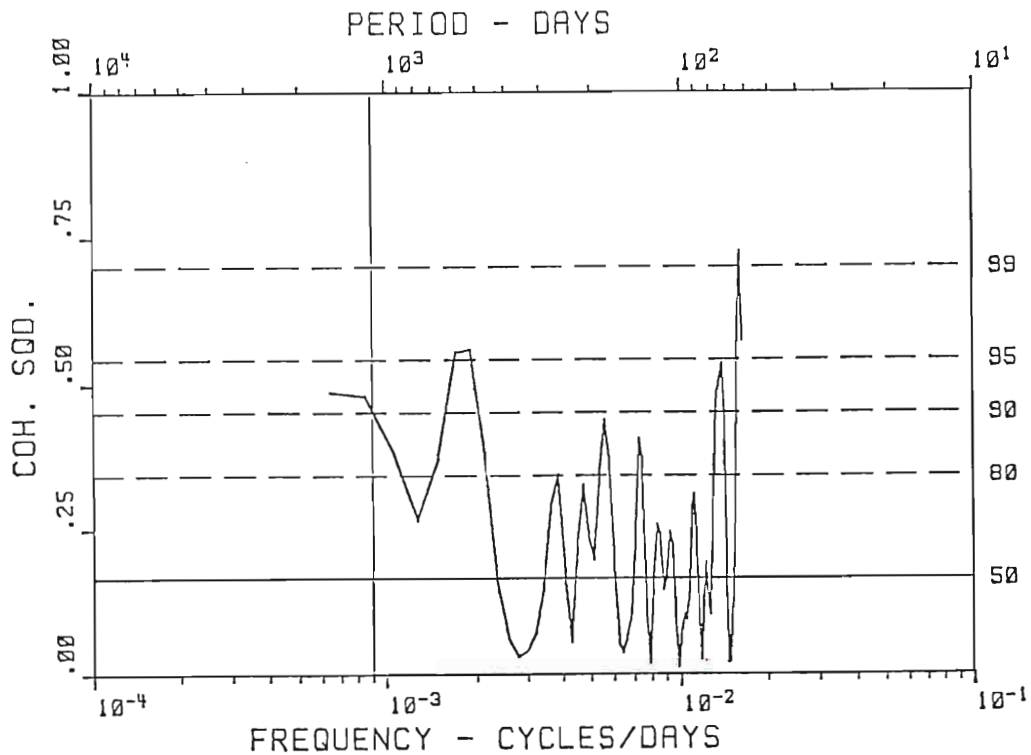


Figure 14. Coherence of the PMC and coastal sea level at San Francisco. Note the 90% or greater coherence in the period band 3-4.4 years. The spectra has been Hanning smoothed, resulting in a loss of coherence values at the frequency extremes.

obtained. The mean phase speed within the projection mode (obtained by dividing the projection mode frequencies (Fig. 13) by k , then averaging) is -1.3 cm sec^{-1} , in agreement with the theoretical phase speed of Rossby waves at 40N.

Using the Rossby wave dispersion relation and the local wavenumbers within the projection mode (obtained from Fig. 12), a theoretical frequency range of -0.5 to -0.25 cycles year $^{-1}$ is obtained, consistent with the frequency range within the projection mode (Fig. 13). The Rossby wave-like features within the projection mode have been shown to be forced at the eastern boundary by coastal Kelvin wave propagation. This finding of coastal Kelvin wave excited Rossby waves at 40N is consistent with the critical latitude (Θ_c) defined by McCreary, et al. (1987), $\Theta_c = \tan^{-1}(c/(2\sigma a))$, where c is the gravity wave phase speed, σ is the frequency and a is the radius of the earth. Equatorward of Θ_c Rossby waves can be excited by coastal Kelvin waves. Using $c=250 \text{ cm sec}^{-1}$ and a mean period of 3 years a critical latitude of 71N is found.

The projection eigenmode accounts for 47.5% of the variance in the 300 meter temperature anomalies. The 47.5% variance explained by the projection mode implies that Rossby waves forced by coastal Kelvin wave propagation account for 47.5% of the variance in 300 meter temperature anomalies for 135W-125W at a latitude of 40N. The implication of this result is that the physical mechanism of the numerical model used in this research accounts for 47.5% of the variance in the temperature anomalies.

numerical model used in this research accounts for 47.5% of the variance in the temperature anomalies.

5. Summary and conclusions

The northern extent of offshore Rossby wave propagation generated by coastal Kelvin waves was addressed by McCreary et al. (1987). McCreary et al. define a critical latitude (Θ_c) which is the northernmost latitude where Rossby waves can be excited by coastal Kelvin wave propagation. In this study a critical latitude of 71N is found. It is then reasonable to expect to see boundary forced Rossby waves at 40N, and in this research the degree to which these waves are present is assessed.

Through the use of PPCA and two data sets, model ULT and 300 meter depth temperature anomalies, a Rossby wave-like signal (projection mode) accounting for 47.5% of the variance in the 300 meter temperature anomalies was obtained. Large amplitude nearshore and decreasing amplitude away from shore implies nearshore generation of these waves. The decrease in amplitude away from shore is evidence of Rossby wave dispersion. The Rossby waves have wavelengths on the order of 1000 km and a majority of their periods between 2 and 4 years. The mean phase speed of the Rossby wave-like features within the projection mode is consistent with the theoretical Rossby wave phase speed at 40N. Effects of the equatorial El Niño events of 1976 and 1982-83 are clearly present in the projection mode, with large associated positive temperature anomalies.

are clearly present in the projection mode, with large associated positive temperature anomalies.

An important source of sea level variability along the west coast of North America at periods of 2-4 years was identified by Pares-Sierra and O'Brien (1989) as poleward propagating Kelvin waves. Since the Rossby waves observed in the projection mode have a majority of their periods ranging between 2 and 4 years, their forcing can be attributed to long period Kelvin waves.

Spectral comparisons between the projection mode's values at 125W and coastal sea level produced greater than 90% coherence in the period band 3-4.4 years. A strong coherence in the period band attributed to coastal Kelvin wave propagation implies a strong relationship between the two. The phases in the period band 3-4.4 years shows that the projection mode lags coastal sea level, suggesting that information is travelling from the coast offshore. The speed at which the information propagates offshore was determined to be a reasonable nearshore Rossby wave phase speed.

It is concluded that the Rossby waves observed in the projection mode are forced by coastal Kelvin waves. This result wasn't totally unexpected, since the model from which the projection mode's structure function was obtained has its Rossby wave-like features forced similarly. These results show a dynamic mechanism for the connection of equatorial El Niño events with north Pacific El Niños, i.e., an oceanic teleconnection.

The nonlinear, reduced gravity $1\frac{1}{2}$ layer model used in this research simulates the oceanic circulation in the northeast Pacific

The nonlinear, reduced gravity $1\frac{1}{2}$ layer model used in this research simulates the oceanic circulation in the northeast Pacific using Kelvin waves propagating along the west coast of North America

as its only forcing. The model has several limitations: no thermodynamics, no bottom topography and 1 baroclinic mode. Even with these limitations, the physical mechanism of this numerical model, and the projection mode, produces results that account for 47.5 % of the variance in 300 meter temperature anomalies.

White and Saur (1983) suggest that the mesoscale variability above 30N is due to predominantly due to wind forced Rossby waves, hence boundary forced Rossby waves are negligible. Our results clearly show that boundary forced Rossby waves are not negligible within the area we examined. On the basis of our result, however, it isn't possible to confirm or deny the conclusion of White and Saur. A 10 degree longitude band is too small to generalize the result to include large scale variability, particularly for large disturbances along the coast.

In addition to the evidence of an oceanic teleconnection, it has also been shown that PPCA is an effective tool in extracting information describing the varying physical attributes (wave number, frequency and amplitude) of propagating features in travelling wave-like fields.

References

- Anderson, D. L. T., and P. W. Rowlands, The role of inertia-gravity and planetary waves in the response of a tropical ocean to the incidence of an equatorial Kelvin wave on a meridional boundary, *J. Mar. Res.*, *34*, 295-312, 1976.
- Barnett, T. P., Interaction of the monsoon and Pacific trade wind system at interannual time scales. Part 1: the equatorial zone. *Mon. Wea. Rev.*, *111*, 756-773, 1983.
- Bendat, J. S., and Piersol, A. G., *Random Data*, 2nd ed., Wiley-Interscience, New York, 1986.
- Camerlengo, A. L., and J. J. O'Brien, Open boundary conditions in rotating fluids, *J. Comput. Phys.*, *35*, 12-35, 1980.
- Clarke, A. J., The reflection of equatorial waves from oceanic boundaries, *J. Phys. Oceanogr.*, *13*, 1193-1207, 1983.
- Emery, W. J., and L. Magaard, Baroclinic Rossby waves as inferred from temperature fluctuations in the Eastern Pacific. *J. Mar. Res.*, *34*, 365-385, 1976.
- Gill, A. E., *Atmosphere - Ocean Dynamics*, Academic Press, San Diego, 1982.
- Inoue, M. I., and J. J. O'Brien, Interannual variability in the tropical Pacific for the period 1979-1982, *J. Geophys. Res.*, *92*, 11,671-11,679, 1987.
- Pacific for the period 1979-1982, *J. Geophys. Res.*, *92*, 11,671-11,679, 1987.

- Johnson, M. A., and J. J. O'Brien, The northeast Pacific Ocean response to the 1982-83 El Niño, accepted for publication in *J. Geophys. Res.- Oceans*, 1989.
- Kubota, M., and J. J. O'Brien, Variability of the upper tropical Pacific Ocean model, *J. Geophys. Res.*, *93*, 13,930-13,940, 1988.
- Legler, D. M., Empirical orthogonal function analysis of wind vectors over the tropical Pacific ocean region, *Bull. Am. Meteorol. Soc.*, *64*, 234-241, 1983.
- McCreary, J. P., P. K. Kundu, and S. Chao, On the dynamics of the California Current system, *J. Mar. Res.*, *45*, 1-32, 1987.
- Moore, D. W., Planetary-gravity waves in an equatorial ocean, PH. D. dissertation, 207 pages, Harvard Univ., Cambridge, Mass., 1968.
- O'Brien, J. J., Using supercomputers to understand and forecast El Niño, I/O, vol. 4, no. 2, 3-7, 1987.
- Pares-Sierra, A. and J. J. O'Brien, The seasonal and interannual variability of the California current system: a numerical model, *J. Geophys. Res.*, *94*, 3,159-3,180, 1989.
- Priesendorfer, R. W., Principle Component Analysis in Meteorology and Oceanography, Elsevier, Amsterdam, 1988.
- Price, J. M. and L. Magaard, Rossby wave analysis of the baroclinic potential energy in the upper 500 meters of the North Pacific, *J. Mar. Res.*, *38*, 249-264, 1980.
- , Rossby wave analysis of subsurface temperature fluctuations along the Honolulu-San Francisco great circle. *J. Phys. Oceanogr.*,
- , Rossby wave analysis of subsurface temperature fluctuations along the Honolulu-San Francisco great circle. *J. Phys. Oceanogr.*, *13*, 258-268, 1983.

- Quinn, W. H. and V. T. Neal, El Niño occurrences over the past four and a half centuries, *J. Geophys. Res.*, *92*, 14,449-14,461, 1987.
- White, W. B., Travelling wave-like mesoscale perturbations in the North Pacific current. *J. Phys. Oceanogr.*, *12*, 231-243, 1982.
- , The resonant response of interannual baroclinic Rossby waves to wind forcing in the eastern midlatitude North Pacific. *J. Phys. Oceanogr.*, *15*, 403-415, 1985.
- White, W. B., and J.F.T. Saur, A source of annual baroclinic Rossby waves in the eastern subtropical North Pacific. *J. Phys. Oceanogr.*, *11*, 1452-1462, 1981.
- , Sources of interannual baroclinic waves in the eastern subtropical North Pacific. *J. Phys. Oceanogr.*, *13*, 531-544, 1983.
- Wyrтки, K., El Niño - The dynamic response of the equatorial Pacific ocean to atmospheric forcing. *J. Phys. Oceanogr.*, *5*, 572-584, 1975.